


Research Article

Stability Analysis of Support Anchor Bolt in the Process of Surrounding Rock Fracture Evolution

Juncai Cao ^{1,2,3,4} Nong Zhang,^{1,2} Liming Pi,³ Tieliang An,^{1,2} Shuchen Li,^{1,2} and Enan Chi⁴

¹State Key Laboratory of Public Big Data, Guizhou University, Guizhou, Guiyang 550025, China

²Key Laboratory of Deep Coal Resource Mining, Ministry of Education of China, School of Mines, China University of Mining and Technology, Xuzhou 221116, China

³Panjiang Coal Power Group Technology Research Institute Co., Ltd., Guizhou, Guiyang 550025, China

⁴Poly Xianlian Blasting Engineer Limited Corp, Guizhou, Guiyang 550002, China

Correspondence should be addressed to Juncai Cao; tb17020001b0@cumt.edu.cn

Received 1 November 2022; Revised 17 January 2023; Accepted 28 March 2023; Published 6 July 2023

Academic Editor: Jinze Xu

Copyright © 2023 Juncai Cao et al. This is an open access article distributed under the Creative Commons Attribution License, which permits unrestricted use, distribution, and reproduction in any medium, provided the original work is properly cited.

Various diseases and failures inevitably appear on expressway roadways in water-rich strata under the long-term erosion of water. It is very difficult to support the surrounding rock of a water-rich roadway because water will corrode the anchorage bond and weaken the surrounding rock mass. In the process of supporting, damage and fracture of anchor bolt often appear in water-rich roadway. In order to study the stability analysis of a support anchor bolt in the process of surrounding rock fracture evolution and the relationship between the prestressed value and the length of the anchor bolt, this paper studied the fracture evolution law of surrounding rock and the progressive debonding law of the bolt are studied by RFPA3D numerical simulation and used MATLAB software to calculate and draw several graphs to reveal the mechanism by analytical method. The following main conclusions were drawn: (1) the change and attenuation of the surrounding rock stress have a certain influence on the stability of the supporting bolt. The existence of confining pressure (horizontal stress) has a significant impact on the ultimate pullout force of anchor bolts. (2) With the gradual destruction of the surrounding rock, the shear stress, horizontal stress, and vertical stress in the surrounding rock are gradually reduced to zero, and the change speed of the surrounding rock is fast at the shallow surface and slow at the deep. (3) The interface shear stress tends to a low stable value after debonding, which means the value of friction resistance is relatively stable in different positions. (4) The frictional resistance after interface debonding is an important condition to maintain the balance of higher anchorage force. If there is no friction resistance, when the axial force of the anchor bolt reaches the initial critical value, the interface debunking process will develop catastrophically and cannot be stabilized until complete failure, even if the axial force no longer increases.

1. Introduction

With the large-scale construction of coal mines in China, the number and mileage of roadways are also developing rapidly. More and more highway roadways are affected by the construction environment, construction conditions, and other factors during roadway operation. Most of the coal mine roadways are located in soft and broken-water-rich strata, and the roadway roof is very prone to instability and collapse under mining disturbance. Roof accidents account for the highest proportion of coal mine safety accidents in China, which seriously threaten the life safety of miners and restrict the efficiency

of coal mining. It is very difficult to support the surrounding rock of water-rich roadway because water will corrode the anchorage bond and weaken the surrounding rock mass [1–3].

As is known to all, the essence of roadway support is to maintain the mechanical balance of the surrounding rock mass within a specified time. In addition, all large deformations and collapses of surrounding rock masses are caused by mechanical imbalances. Moreover, the mechanical balance state of the surrounding rock is dynamically changing, and these changes are related to the rheology time of the surrounding rock mass. Anchor support is one of the most direct ways to maintain mechanical balance. Since its invention, the anchor, or cable,

has been employed to solve challenging support problems in mining engineering and its related disciplines. Anchors have the advantages of low cost, good support effect, and flexible operation, and thus they are widely used [4–6]. The installation styles for the anchor are divided into partial anchoring and full-length anchoring, and partial anchoring can be applied to an anchor prestress. The prestressed anchor support can directly prevent the premature cracking of the surrounding rock of the roadway and, at the same time, mobilize the rock mass to participate in the carried in time. Thus, the anchor support can greatly slow the deterioration process of the surrounding rock and keep the roof safe and stable [7, 8]. Although many researchers have done a lot of research on prestressed anchor, the method to determine the parameters of prestressed anchor bolt support is still not mature because its dynamic failure process is complex and the corresponding research methods have various limitations.

The physical model test is an important means to study the mechanisms and characteristics of an anchor support. The model test can visually and intuitively simulate the whole process of force, deformation, and damage of the engineering structure and can simulate the complex geology more comprehensively and the support structure more realistically [9–11]. Although the physical model can simulate the failure process of the anchor, it is unfortunate that the damage process inside the model cannot be seen and captured, and repeating the physical experiment is difficult. Moreover, the theory of physical similarity simulation is still immature, especially regarding the research and selection of similar materials. The most important issue is that physical model testing is also difficult and inconvenient when studying the impact of time on anchor supports.

Numerical calculation is another important method for studying the mechanisms and characteristics of anchor supports. Numerical tests are repeatable and flexible. In geotechnical engineering, common numerical software includes FLAC3D, 3DEC, PFC3D, ABAQUS, and ANSYS [12–15]. As engineering challenges continue to escalate and computational requirements continue to increase, the limitations of these softwares are increasingly exposed. There are two main limitations. On the one hand, the number of cells in the calculation model cannot be excessively divided; otherwise, the calculation speed may slow, or calculations may cease due to memory requirements that exceed the capacity of the computer. For example, a 3D model with a size of $600\text{ m} \times 300\text{ m} \times 1000\text{ m}$ is divided into millions of cells and takes several days to perform an elastoplastic analysis using a finite element method. When the number of cells exceeds 10 million, the 3D model can barely be calculated by computer, especially for the related rheological model. On the other hand, the number of cells in the calculation model cannot be too small, or the results of the calculation will be incorrect or not meet accuracy requirements. Although science, technology, and computer performance are constantly improving, the speed of computer development is far from meeting the requirements of certain large engineering projects. In addition, like the physical model test, it is also difficult to study the impact of time on anchor supports.

The theoretical analytical method is a supplement to the numerical simulation method. Combining theoretical analysis

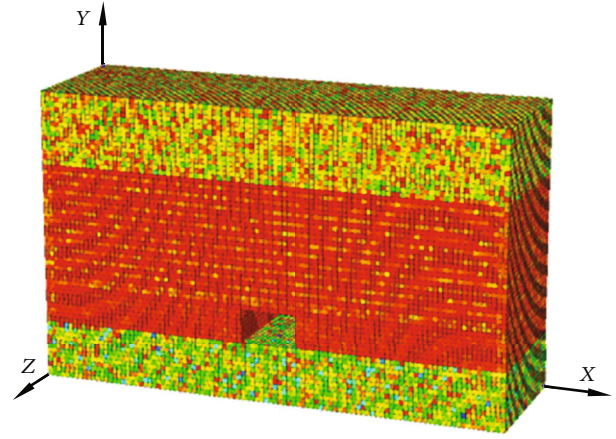


FIGURE 1: The calculation model of failure law.

and numerical simulation, the stability of a support anchor bolt in the process of surrounding rock fracture evolution is analyzed in this paper.

2. Stress Law in the Process of Fracture Evolution of Surrounding Rock

The surrounding rock in the process of fracture evolution shows strong timeliness. Due to the limitation of monitoring technology, only the displacement and bearing stress of the surrounding rock surface are monitored on site. It is difficult to capture the law of stress evolution in the surrounding rock. In this chapter, the stress evolution law in the process of roadway surrounding rock fracture is studied through RFPA-3D numerical simulation, and the calculation model is shown in Figure 1. The model size is $40000 \times 24 \times 14000\text{ mm}$, and the height and width of the roadway are 2800 mm and 4800 mm , respectively. The simulation load gradually increases from 2 MPa of confining pressure to 30 MPa until the surrounding rock of the roadway is destroyed and the simulation is terminated.

The mechanical parameters of the numerical model are shown in Table 1. The material parameters of the similar model and the numerical model are set according to the similar proportion of the physical model principle. By considering the engineering conditions and the frame size, the geometrical and mechanical similarity ratios were determined: $CL = 1:20$, $C\rho = 1:1.6$, and $C = 1:100$ (CL is the constant of geometry similarity, $C\rho$ is the constant of density similarity, and C is the constant of stress similarity).

The numerical model and the physical model maintain the consistency of material properties, but there is no uniform requirement for the loading force, which is gradually loaded from zero until the model is destroyed. Figure 2 shows the law of change and evolution of numerical simulation and physical simulation. The maximum displacement of the physical model after failure is 72 mm . Compared with the initial state of 160 mm , the roof subsidence is 45% ; However, the maximum displacement of the numerical model after failure is 1.24 m , which is 44.2% lower than the initial 2.8 m . The results show that the roof deformation and shrinkage rate of both of them reached about 45% in the roadway. In addition, both of them show fracture arch shape

TABLE 1: Mechanical parameters of rock and coal of numerical model.

Rock properties	Density ($\text{kg}\cdot\text{m}^{-3}$)	E (MPa)	μ	Compressive strength (MPa)	Thickness (m)	Φ ($^\circ$)
Sandstone	2760	28000	0.14	105.2	6.7	35
M8 coal	1350	500	0.2	15	0.5	25
Siltstone with mud	2690	18000	0.16	41.4	6	32
Carbonaceous mudstone	1650	600	0.24	16	0.5	25
Siltstone with mud 2	2680	4000	0.18	35	4.5	30
M9 coal	1800	1440	0.20	20	2.8	25
Siltstone	2800	8000	0.14	95.2	6	35

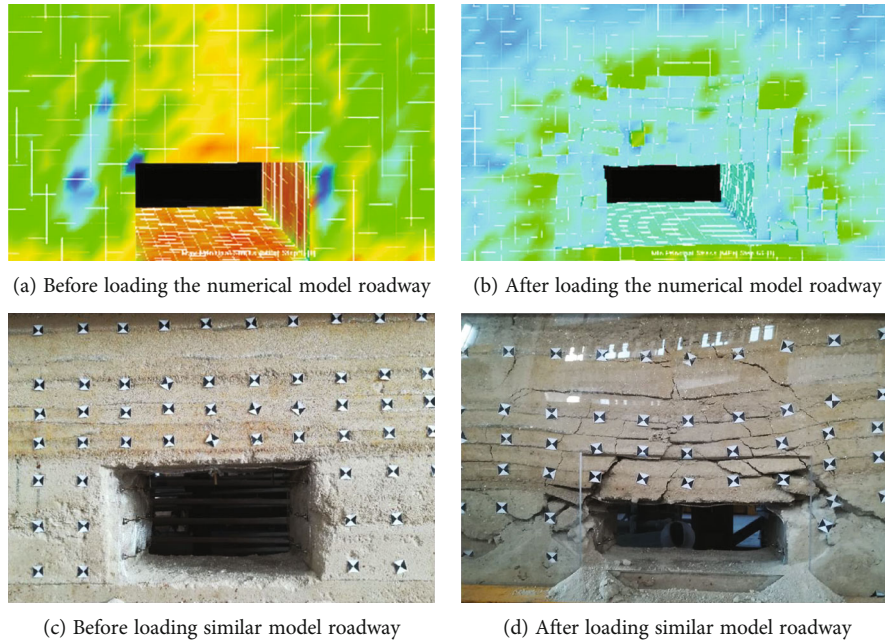


FIGURE 2: Comparison test of numerical model and similar model results.

after loading failure of the roadway surrounding rock, and their fracture shape and characteristics are highly consistent. Therefore, the numerical simulation is consistent with the physical model failure, and the use of numerical simulation fracture evolution data information can reveal the stress evolution law in the process of surrounding rock fracture.

Figure 3 shows the failure process and stress evolution law of the roadway surrounding rock. Figure 3(a) shows the fracture evolution process of the surrounding rock; Figure 3(b) shows the stress curves of surrounding rock at different positions within 1m of the roadway roof; Figure 3(c) shows the stress curves of surrounding rock at different positions within 2.5 m of the roadway roof; and Figure 3(d) shows the stress curves of surrounding rock at different positions within 4 m of the roadway roof. The research results on shear stress show that, in the initial state, the peak shear stress at 1 m of the above roof is 3 MPa, the peak shear stress at 2.5 m of the roof is 1.5 MPa, and the peak shear stress at 4 m of the roof is 1.0 MPa. The peak shear stress in the roof gradually decreases from the surface to the inside. With the gradual increase of surrounding rock stress, the peak shear stress also gradually increases (3 MPa to 7.5 MPa of the roof 1 m). When the peak

shear stress exceeds the shear strength of the surrounding rock, the surrounding rock will be destroyed, and the peak shear stress will decrease accordingly. With the progressive destruction of the surrounding rock, the shear stress value gradually tends to zero. This trend occurs gradually from the outside to the inside. The research results of horizontal stress (X direction) show that, in the initial state, the horizontal stress (X direction) at different positions of the 1 m roof is evenly distributed, and the horizontal stress at different positions tends to about 4 MPa. The horizontal stress curve of the roof at 2.5 and 4 m inside the roof is basically consistent with that at 1 m. With the gradual increase of surrounding rock stress, the horizontal stress values at different positions (1, 2.5, and 4 m in the roof) in the vertical direction also gradually increase (4 MPa to 10 MPa); When the horizontal stress exceeds the strength of the surrounding rock, the surrounding rock will be damaged, and the horizontal stress will decrease accordingly; With the progressive destruction of the surrounding rock, the horizontal stress gradually tends to zero; This trend occurs gradually from the outside to the inside. The research results on vertical stress (Y direction) show that the vertical stress distribution in different layers (1, 2.5, and

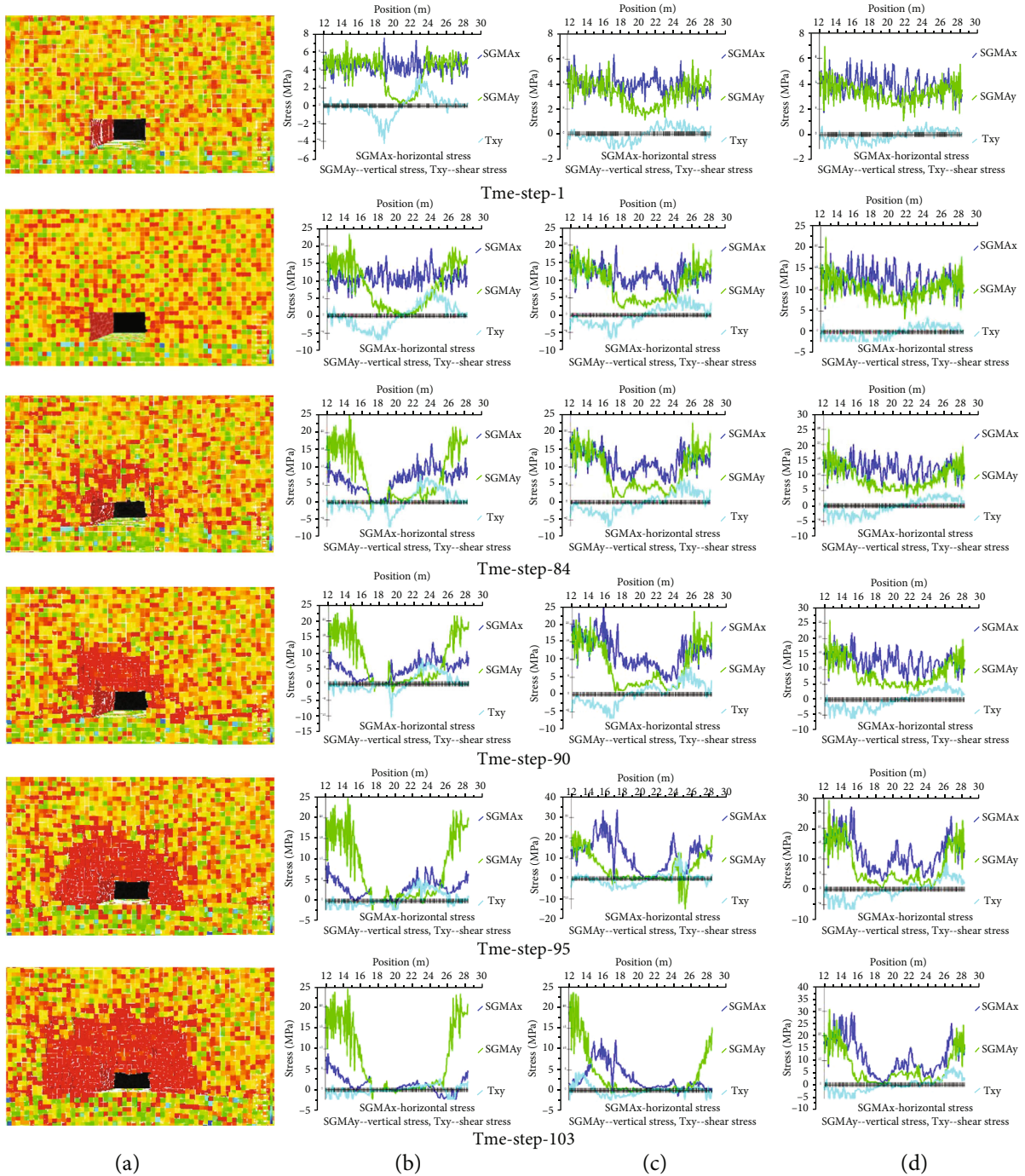


FIGURE 3: The failure law and stress changing law of the surrounding rock.

4 m in the roof) is obviously different from the horizontal stress. In the initial state, at the 1 m layer of the roof, the vertical stress in the middle of the roadway is close to zero, and the vertical stress on both sides of the roadway gradually increases. Compared with 1 m in the roof, the minimum vertical stress at 2.5 m in the roof becomes 1.8 MPa, and the minimum vertical stress at 4 m in the roof becomes 2.2 MPa. With the progressive destruction of the surrounding rock, the vertical stress decreases as a whole, and the vertical stress at different positions in the horizontal direction gradually tends to zero from the middle to both sides. This trend occurs gradu-

ally from the outside to the inside. In a word, with the gradual destruction of the surrounding rock, the shear stress, horizontal stress, and vertical stress in the surrounding rock are gradually reduced to zero, and the change speed of the surrounding rock is fast at the shallow surface and slow at the deep. Before the failure of the surrounding rock, the stress of the surrounding rock will increase with the increase in buried depth. In the process of progressive failure and damage of the surrounding rock, the stress field gradually shifts to the deep part and both sides of the roadway. The values of vertical stress, horizontal stress, and shear stress of the surrounding rock within the

scope of damage gradually decrease. This law is helpful to analyze the stress state of anchor bolts at different stages and to guide the safety control of anchor support.

3. The Progressive Debonding Process of Anchor Based on Numerical Simulation

The change and attenuation of the surrounding rock stress have a certain influence on the stability of the supporting anchor bolt. In this chapter, RFPA-3D software is used to study the evolution law of the anchor drawing fracture process. The matrix size of the numerical model concrete is 180 mm × 180 mm × 400 mm, the diameter of the bolt is 20 mm, the length is 330 mm, the exposure is 30 mm, and the interface thickness of the anchorage agent is 2 mm. The loading mode takes displacement as a variable, and the loading step is 0.01 mm. The strength of the rock matrix is 50 MPa, and the elastic modulus is 10000 MPa. The strength and elastic modulus of the anchorage agent are 30 MPa and 7000 MPa, respectively. The strength and elastic modulus of the bolt are 1400 MPa and 210000 MPa, respectively. The bottom end of the model matrix was fixed, and the anchor rod was pulled by external force, as shown in Figure 4 for the specific model.

3.1. Failure Analysis of Anchor Drawing Process. The fracture process of the anchorage interface is shown in Figure 5. The step in the figure represents the load step in the finite element calculation. It can be seen from Figure 5(a) that, at the initial stage of loading (step 1, 18 kN), no obvious failure occurs in the model, and the drawing stress of the anchor is mainly concentrated in the outcrop of the anchor. With the increase in load (step 2, Figure 5(b)), the damage element first appears at the embedded end of the bolt (that is, the exposed end of the bolt is in the rock matrix) and the nearby anchorage interface, and the anchorage interface is partially debonded and fails. This is because the stiffness, strength, and other mechanical parameters of the anchor-interface-matrix differ greatly, which leads to the uncoordinated deformation. Then, the anchorage interface unit will be damaged immediately after its strength exceeds the damage threshold. As the load continues to increase (step 3~step 12, Figures 5(c)–5(j)), the cracks in the anchorage interface continue to expand from the surface to the inside until the interface is completely debonded. When the anchor is completely debonding failure, the ultimate drawing force of the anchor bolt is about 220 kN.

3.2. Evolution Analysis of Acoustic Emission. Acoustic emission (AE) is a nondestructive detection method, which can effectively locate the position of material during damage and detect the energy release of components during damage. By studying the evolution process of acoustic emission, the evolution law of crack propagation in the material can be effectively revealed. Figure 6 clearly shows the acoustic emission spatiotemporal evolution diagram of the RFPA3D software, and the pink bubbles represent shear failure and the blue bubbles represent tensile failure. At the initial stage of loading, the pulling force is small and no AE occurs in the model (step 1), indicating that the anchorage interface is stable and no damage occurs. With the gradual increase of

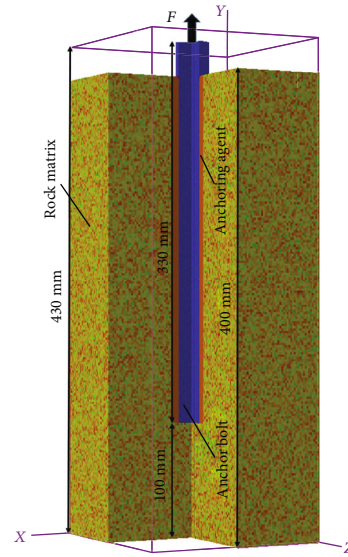


FIGURE 4: 3D section view of drawing model of anchor.

the pulling force, the acoustic emission first appeared near the outcrop of the anchor, and no obvious acoustic emission bubbles were generated inside the model. At this time, the anchoring interface of the acoustic emission position is debonded and destroyed. The type of damage includes tensile failure and shear failure, but the tensile failure is significant at the initial stage of loading (step 2). As the loading continues, the AE bubbles along the interface of the anchor appear continuously. Compared with the AE bubbles near the outcrop, the AE bubbles at the internal interface are small and dense; at this time, the shear failure gradually dominates (step 3–step 12). At the later stage of loading, AE bubbles have been filled all around the anchorage interface, indicating that the interface is all debonded. The results show that AE evolution is a gradual process during anchor drawing, and so is bubble development. The main cause of interface debonding is shear failure, followed by tensile failure; however, it is worth noting that the essence of shear debonding is tensile failure on the maximum shear plane.

3.3. Evolution Law of Axial Force and Interface Shear Stress of Anchor. Figure 7(a) shows the changes in the anchor axial force at different positions and loading steps. In this part, the variation law of shear stress during anchor bolt drawing is studied. At the early stage of loading, the axial force curve of the bolt is relatively gentle (step 1), and the pulling force of the anchor bolt is about 18 kN. As the loading step goes on, the drawing force of the experiment increases gradually, and the axial force of the bolt at different positions also increases (step 2~step 12). The variation of axial force also reflects the debonding process of the anchorage interface. During the experiment, the sum of shear force and frictional resistance at the debonding position of the anchorage interface should be balanced with the pulling force of the anchor. Anchorage interfaces without debonding provide shear resistance. The debonded anchorage interface provides friction resistance. Therefore, the difference between shear resistance or friction resistance and the anchor bolt drawing force is the anchor

axial force at different positions. The continuous increase in drawing force leads to the constant debonding of the interface. At the same time, the axial force of the anchor bolt is constantly adjusted, and the shear force and frictional resistance of the anchorage interface continue to increase until the anchor bolt is completely debonded and fails. Figure 7(b) shows the shear stress variation law of anchorage interface and surrounding rock interface. Similarly, the shear stress without the debonding part is shear resistance, while the shear stress of the debonding part is friction resistance. In the shear stress curve, the position near the peak value is the debonding position. The right side of the peak represents debonding, and the left side represents undebonding. The shear stress curve also vividly shows the progressive debonding process of the anchor (step 1~step 12). The results show that the interface shear stress tends to a low stable value after debonding, which means the value of friction resistance is relatively stable in different positions.

3.4. The Relationship between Surrounding Rock Stress and Anchorage Interface Debonding. Based on the anchor bolt pullout model above, the failure process and ultimate pullout force of the bolt under four different confining pressures of 0, 0.1, 0.6, and 1.1 MPa are studied. Figure 8 shows the displacement change curve of the anchor bolt and anchorage interface under different confining pressures; when the displacement difference between the two is large, it is considered that the anchorage interface debonding failure. When the pullout force is 18 kN, the anchorage interface under the four surrounding rock conditions is not debonded; when the pull-out force is 118 kN, the anchorage interface with a confining pressure of 0 MPa is about 100 mm debonded, the anchorage interface with a confining pressure of 0.1 MPa is about 60 mm debonded, the anchorage interface with a confining pressure of 0.6 MPa is about 45 mm debonded, and the anchorage interface with a confining pressure of 1.1 MPa is about 30 mm debonded; When the pull-out force is 220 kN, the anchorage interface with a confining pressure of 0 MPa is completely debonded (300 mm), the anchorage interface with a confining pressure of 0.1 MPa is

about 170 mm, the anchorage interface with a confining pressure of 0.6 MPa is about 120 mm, and the anchorage interface with a confining pressure of 1.1 MPa is about 80 mm. The results show that the existence of confining pressure (horizontal stress) has a significant impact on the ultimate pullout force of anchor bolts, and the higher the confining pressure is, the greater the ultimate pullout force is.

3.5. The Influence of Surrounding Rock Fracture Process on Bolt Support. With the change of time, the surrounding rock of the roadway will gradually damage and fracture [16–20], leading to gradual debonding of the anchorage interface. The gradual debonding of the anchorage interface will affect the stability of the bolt support and endanger the safety of the support. With the increase in mine burial depth, the fracture range of surrounding rock will increase, leading to a large range of debonding and full debonding of the anchorage interface, with a higher hazard level. Because of the heterogeneity of the surrounding rock and the asymmetry of the load, the fracture process of the surrounding rock also presents an irregular shape, and the anchoring interface debonding law is difficult to unify. This aspect needs to continue to be studied through statistical mechanics and other methods. Bolt prestress is one of the effective ways to eliminate or alleviate this problem. Selecting appropriate bolt prestress is of great help to the stability of supporting surrounding rock. Prestress can slow down the damage and destruction speed of surrounding rock, thereby slowing down the debonding speed of the anchor interface and maintaining the safety of the roadway roof. The appropriate prestress parameters will be discussed below.

4. The Key Support Indexes Analysis of Anchor Based on Analytical Solution

The analytical solution for the anchor consists of two parts: the bonding part and the tray part [21], as shown in Figure 1. The analytical solution for a single anchor on the surrounding rock is as follows [22–25]:

$$\begin{aligned}
 \sigma_z^A(x, y, z) = & \frac{P(z)}{8\pi d^2 - 2\pi^2 r_b^2} \left\{ \arctan \frac{(x+d)(y+d)}{z\sqrt{(x+d)^2 + (y+d)^2 + z^2}} - \arctan \frac{(x+d)(y-d)}{z\sqrt{(x+d)^2 + (y-d)^2 + z^2}} + \arctan \frac{(x-d)(y-d)}{z\sqrt{(x-d)^2 + (y-d)^2 + z^2}} \right. \\
 & - \arctan \frac{(x+d)(y+d)}{z\sqrt{(x-d)^2 + (y+d)^2 + z^2}} + \frac{z(x+d)(y+d)[(x+d)^2 + (y+d)^2 + 2z^2]}{[(x+d)^2 + z^2][(y+d)^2 + z^2]\sqrt{(x+d)^2 + (y+d)^2 + z^2}} - \frac{z(x+d)(y-d)[(x+d)^2 + (y-d)^2 + 2z^2]}{[(x+d)^2 + z^2][(y-d)^2 + z^2]\sqrt{(x+d)^2 + (y-d)^2 + z^2}} \\
 & \left. + \frac{z(x-d)(y-d)[(x-d)^2 + (y-d)^2 + 2z^2]}{[(x-d)^2 + z^2][(y-d)^2 + z^2]\sqrt{(x-d)^2 + (y-d)^2 + z^2}} - \frac{z(x-d)(y+d)[(x-d)^2 + (y+d)^2 + 2z^2]}{[(x-d)^2 + z^2][(y+d)^2 + z^2]\sqrt{(x-d)^2 + (y+d)^2 + z^2}} \right\} \\
 & + \frac{P_0 \alpha}{8\pi(1-\mu_s)} \left\{ \int_{z_0}^{z_0+L} \frac{(1-2\mu)(\omega-z)(e^{\alpha\omega-\alpha z_0} + e^{\alpha z_0-\alpha\omega+2\alpha L})}{(1-e^{2\alpha L})[x^2+y^2+(z-\omega)^2]^{5/2}} d\omega - \int_{z_0}^{z_0+L} \frac{(1-2\mu)(z-\omega)(e^{\alpha\omega-\alpha z_0} + e^{\alpha z_0-\alpha\omega+2\alpha L})}{(1-e^{2\alpha L})[x^2+y^2+(z+\omega)^2]^{5/2}} d\omega \right. \\
 & - \int_{z_0}^{z_0+L} \frac{3(z-\omega)^3(e^{\alpha\omega-\alpha z_0} + e^{\alpha z_0-\alpha\omega+2\alpha L})}{(1-e^{2\alpha L})[x^2+y^2+(z-\omega)^2]^{7/2}} d\omega - \int_{z_0}^{z_0+L} \frac{3(3-4\mu)z(z+\omega)^2(e^{\alpha\omega-\alpha z_0} + e^{\alpha z_0-\alpha\omega+2\alpha L})}{(1-e^{2\alpha L})[x^2+y^2+(z+\omega)^2]^{7/2}} d\omega + \int_{z_0}^{z_0+L} \frac{3\omega(z+\omega)(5z-\omega)(e^{\alpha\omega-\alpha z_0} + e^{\alpha z_0-\alpha\omega+2\alpha L})}{(1-e^{2\alpha L})[x^2+y^2+(z+\omega)^2]^{3/2}} d\omega \\
 & \left. - \int_{z_0}^{z_0+L} \frac{30z\omega(z+\omega)^3(e^{\alpha\omega-\alpha z_0} + e^{\alpha z_0-\alpha\omega+2\alpha L})}{(1-e^{2\alpha L})[x^2+y^2+(z+\omega)^2]^{3/2}} d\omega \right\}, \tag{1}
 \end{aligned}$$

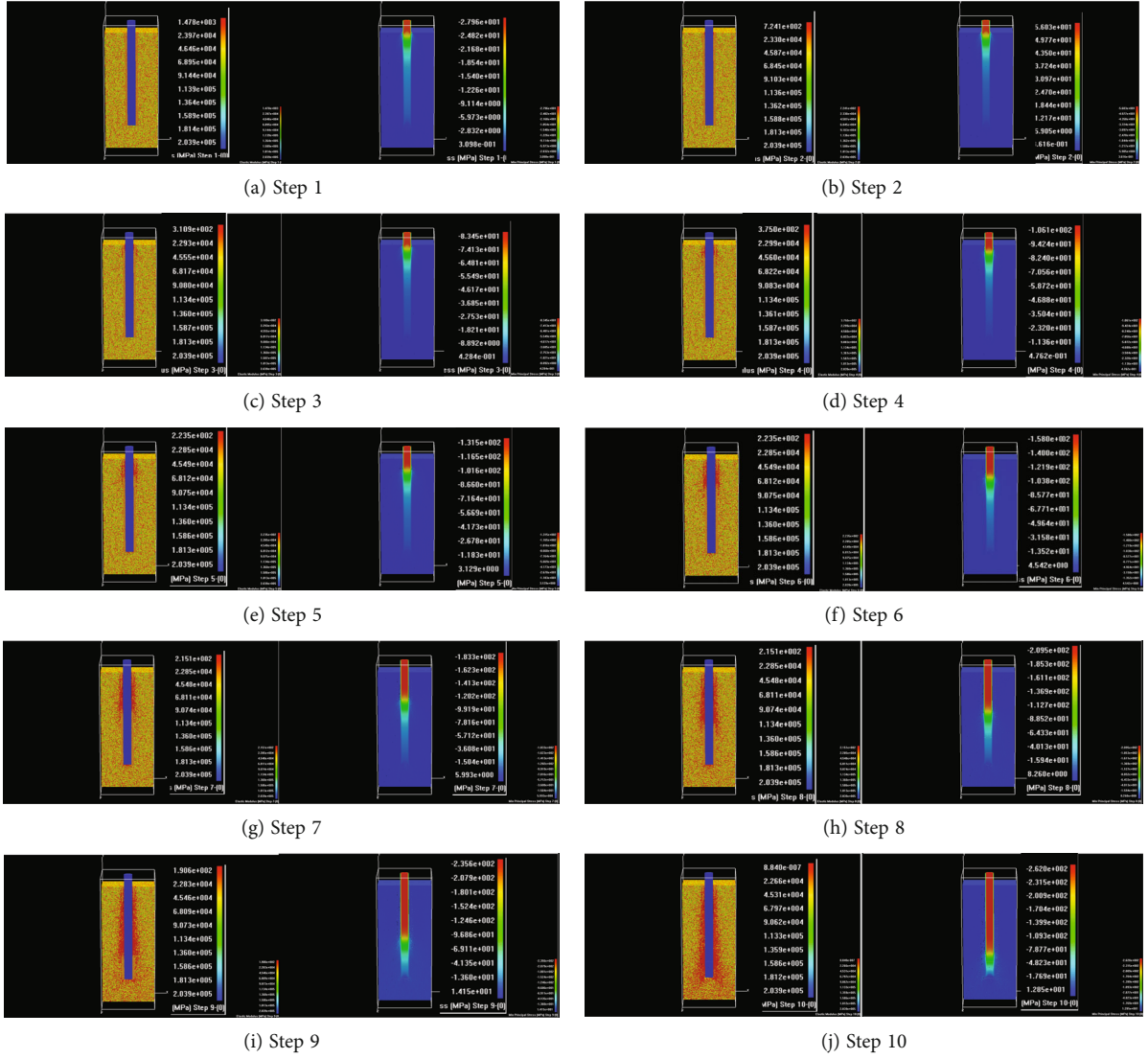


FIGURE 5: Debonding failure process of anchor rod drawing.

where d is the side length of the tray, P_0 is the prestress of the anchor, z_0 is the length of the free section of the anchor, and L is the length of the bonding section of the anchor. The corresponding analytical solutions have been given [26, 27], and the results are as follows:

$$P(z) = P_0(e^{\alpha w - \alpha z_0} - e^{\alpha z_0 - \alpha w + 2\alpha L})(1 - e^{2\alpha L})^{-1}, \quad (2)$$

where $P(z)$ is the anchor axial force of the bonding part at the z position, and P_0 is the initial prestress of the anchor. Using the shear-lag method [28] and the related test results [29], the analytical expression for α is organized as follows:

$$\alpha = \sqrt{\frac{E_m E_g}{\left[E_m (1 + \mu_g) \ln (r_g / r_b) + E_g (1 + \mu_m) \ln (20 E_b r_b / ((E_b + E_m) r_g)) \right] r_b E_b}}, \quad (3)$$

where E_g is the elastic modulus of the surrounding rock, E_m is the elastic modulus of the anchoring agent, E_b is the elastic modulus of the anchor, r_b is the radius of anchor, r_g is the radius of the anchor mounting hole, μ_m is Poisson's ratio of the surrounding rock, μ_g is Poisson's ratio of the anchoring agent, and μ_b is Poisson's ratio of the anchor.

Based on equation (1), the vertical and horizontal stress matrices of the anchor are as follows:

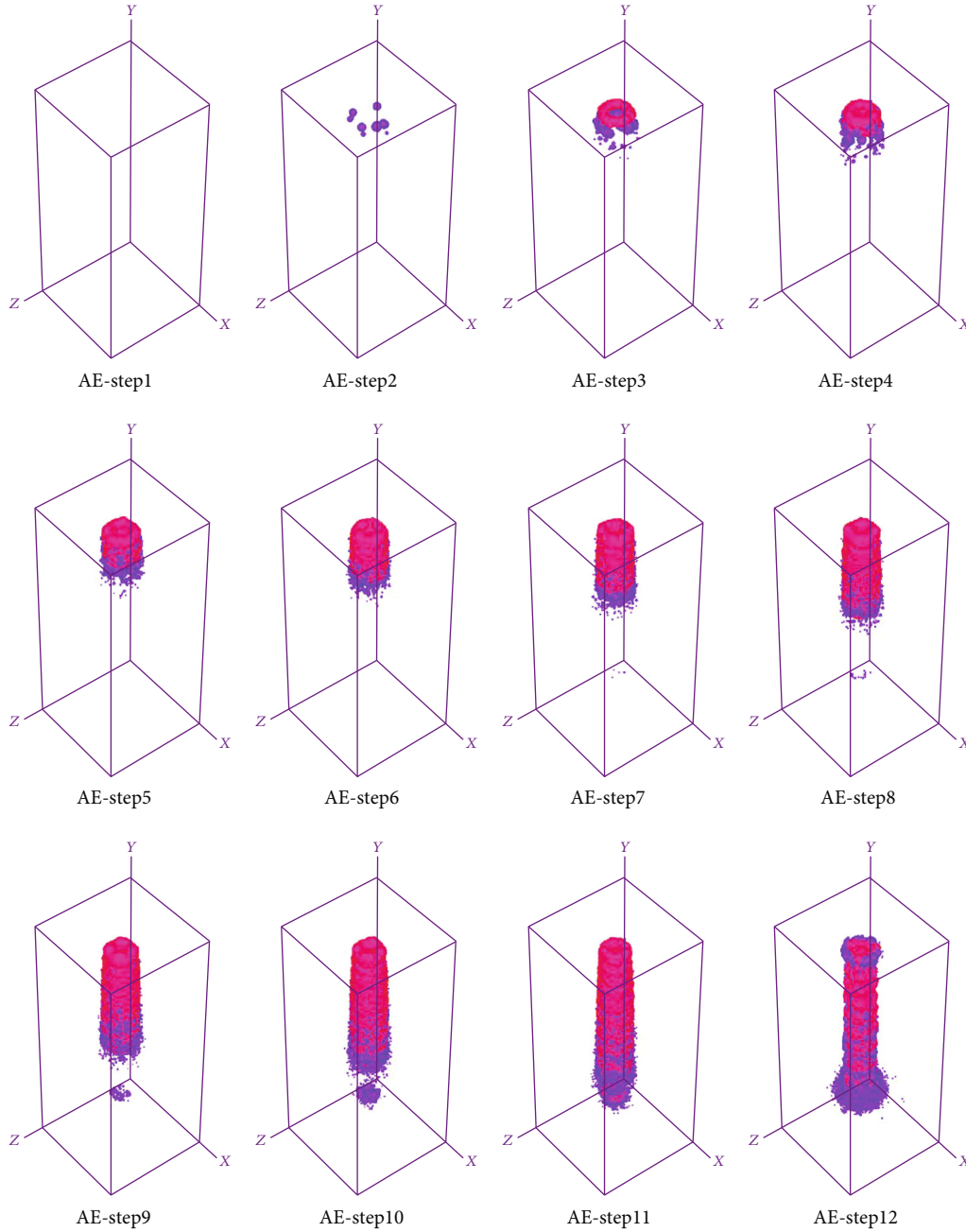


FIGURE 6: Acoustic emission process of anchor rod drawing.

where A_t is the vertical distance from the t -th anchor to the yo z plane and B_w is the vertical distance from the w -th anchor to the xo z plane in the Cartesian coordinate system.

When some M_{an} are superimposed, the coupling stress matrix of anchors on the surrounding rock can be obtained, and its calculation equation is as follows.

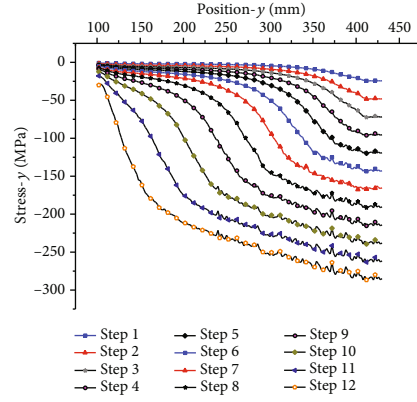
M_{to}^V of the vertical stress matrix is

$$M_{to}^V = M_{su}^V(x, y, z) + M_{\sigma}^V(x, y, z, B_1) + M_{\sigma}^V(x, y, z, B_2) + \dots + M_{\sigma}^V(x, y, z, B_w). \quad (4c)$$

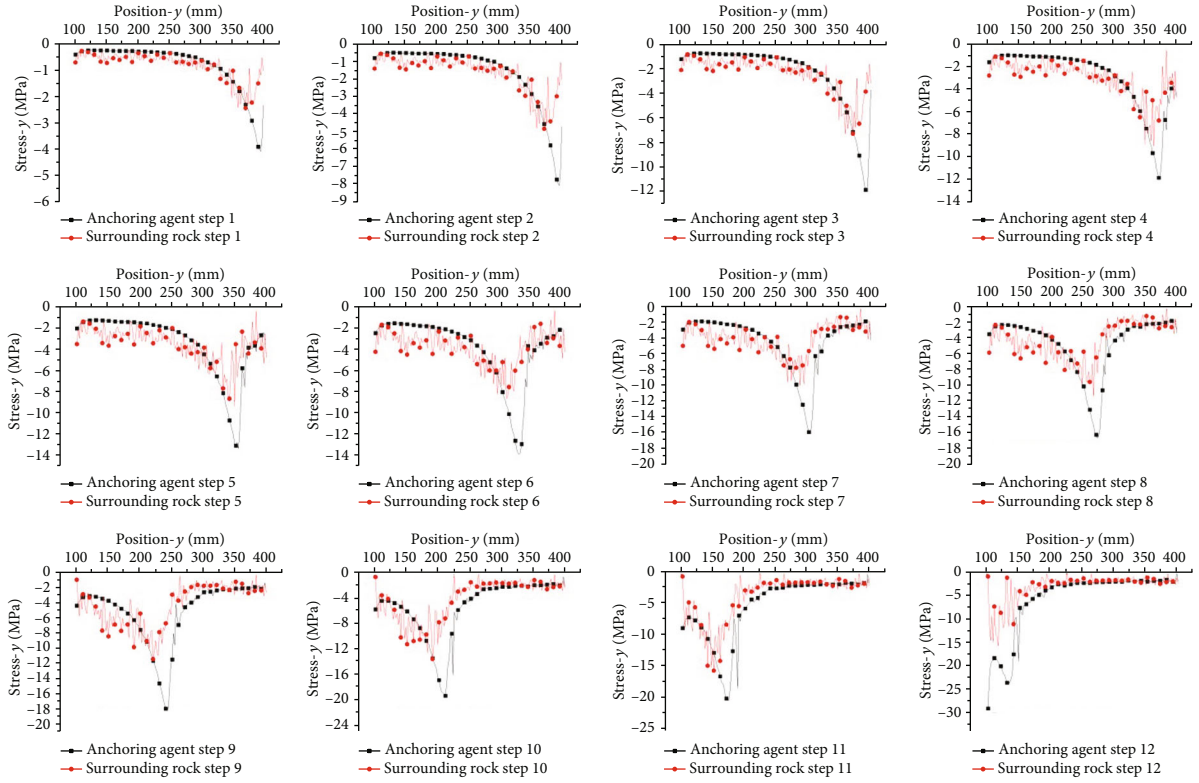
M_{to}^H of the horizontal stress matrix is

$$M_{to}^H = M_{su}^H(x, y, z) + M_{\sigma}^H(x, y, z, A_1) + M_{\sigma}^H(x, y, z, A_2) + \dots + M_{\sigma}^H(x, y, z, A_t), \quad (4d)$$

where $M_{su}^V(x, y, z)$ and $M_{su}^H(x, y, z)$ are the stress matrices of the surrounding rock self in the vertical and horizontal directions, respectively. Based on equation (6), their matrix



(a) The anchor axial force at different positions and loading steps



(b) The shear stress variation law of anchorage interface and surrounding rock interface

FIGURE 7: Stress change analysis of bolt drawing model.

$$M_{an}^H(x, y, z, A_t) = \begin{bmatrix} \sigma_z^A(x_1 - A_t, y_1, z_1) & \sigma_z^A(x_2 - A_t, y_1, z_1) & \cdots & \sigma_z^A(x_n - A_t, y_1, z_1) \\ \sigma_z^A(x_1 - A_t, y_2, z_1) & \sigma_z^A(x_2 - A_t, y_2, z_1) & \cdots & \sigma_z^A(x_n - A_t, y_2, z_1) \\ \vdots & \vdots & \ddots & \vdots \\ \sigma_z^A(x_1 - A_t, y_m, z_1) & \sigma_z^A(x_2 - A_t, y_m, z_1) & \cdots & \sigma_z^A(x_n - A_t, y_m, z_1) \end{bmatrix}, \quad (4a)$$

$$M_{an}^V(x, y, z, B_w) = \begin{bmatrix} \sigma_z^A(x_1, y_1 - B_w, z_1) & \sigma_z^A(x_2, y_1 - B_w, z_1) & \cdots & \sigma_z^A(x_n, y_1 - B_w, z_1) \\ \sigma_z^A(x_1, y_1 - B_w, z_2) & \sigma_z^A(x_2, y_1 - B_w, z_2) & \cdots & \sigma_z^A(x_n, y_1 - B_w, z_2) \\ \vdots & \vdots & \ddots & \vdots \\ \sigma_z^A(x_1, y_1 - B_w, z_i) & \sigma_z^A(x_2, y_1 - B_w, z_i) & \cdots & \sigma_z^A(x_n, y_1 - B_w, z_i) \end{bmatrix}, \quad (4b)$$

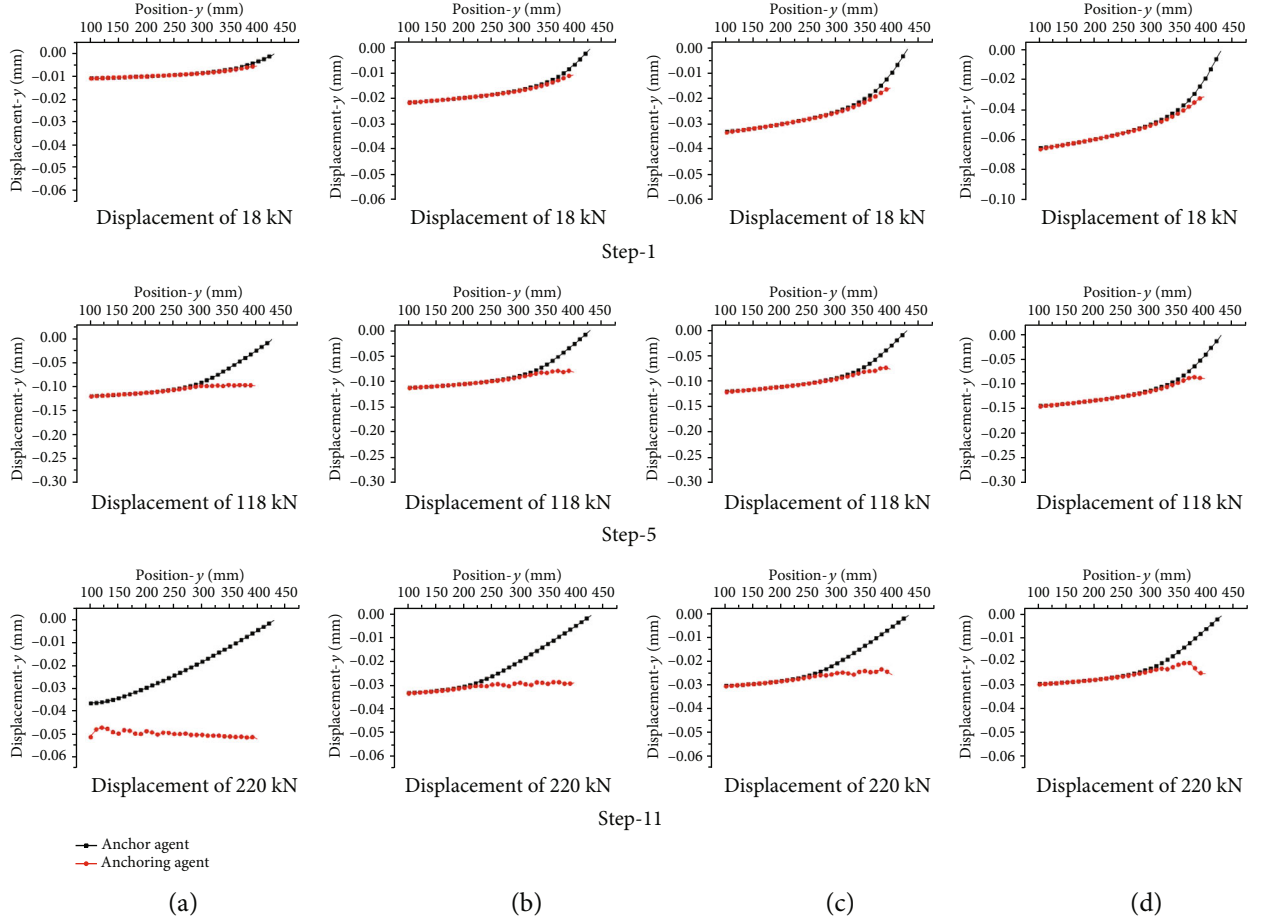


FIGURE 8: Drawing process curve of anchor rod under different confining pressure.

TABLE 2: Pending parameters for the calculation equation.

Name	$L_t = z_0 + L$	d	z_0	L	P_{01}	P_{02}	P_{03}	P_{04}	P_{05}
Anchor	4 m	0.25 m	2 m	2 m	200 kN	500 kN	1000 kN	1500 kN	2000 kN
Anchor	5 m	0.25 m	2 m	3 m	200 kN	500 kN	1000 kN	1500 kN	2000 kN
Anchor	6 m	0.25 m	2 m	4 m	200 kN	500 kN	1000 kN	1500 kN	2000 kN
Name	r_b	r_g	E_g	E_m	E_b	μ_m	μ_g	μ_b	
Anchor	0.015 m	0.0225 m	35 MPa	45 MPa	210 MPa	0.25	0.25	0.3	

expressions are as follows:

$$M_{su}^V(x, y, z) = \begin{bmatrix} \sigma_z^s(x_1, y_1, z_1) & \sigma_z^s(x_2, y_1, z_1) & \cdots & \sigma_z^s(x_n, y_1, z_1) \\ \sigma_z^s(x_1, y_2, z_1) & \sigma_z^s(x_2, y_2, z_1) & \cdots & \sigma_z^s(x_n, y_2, z_1) \\ \vdots & \vdots & \ddots & \vdots \\ \sigma_z^s(x_1, y_m, z_1) & \sigma_z^s(x_2, y_m, z_1) & \cdots & \sigma_z^s(x_n, y_m, z_1) \end{bmatrix}, \quad (4e)$$

$$M_{su}^H(x, y, z) = \begin{bmatrix} \sigma_z^s(x_1, y_1, z_1) & \sigma_z^s(x_2, y_1, z_1) & \cdots & \sigma_z^s(x_n, y_1, z_1) \\ \sigma_z^s(x_1, y_1, z_2) & \sigma_z^s(x_2, y_1, z_2) & \cdots & \sigma_z^s(x_n, y_1, z_2) \\ \vdots & \vdots & \ddots & \vdots \\ \sigma_z^s(x_1, y_1, z_l) & \sigma_z^s(x_2, y_1, z_l) & \cdots & \sigma_z^s(x_n, y_1, z_l) \end{bmatrix}, \quad (4f)$$

When the matrix of surrounding rock self is zero, the

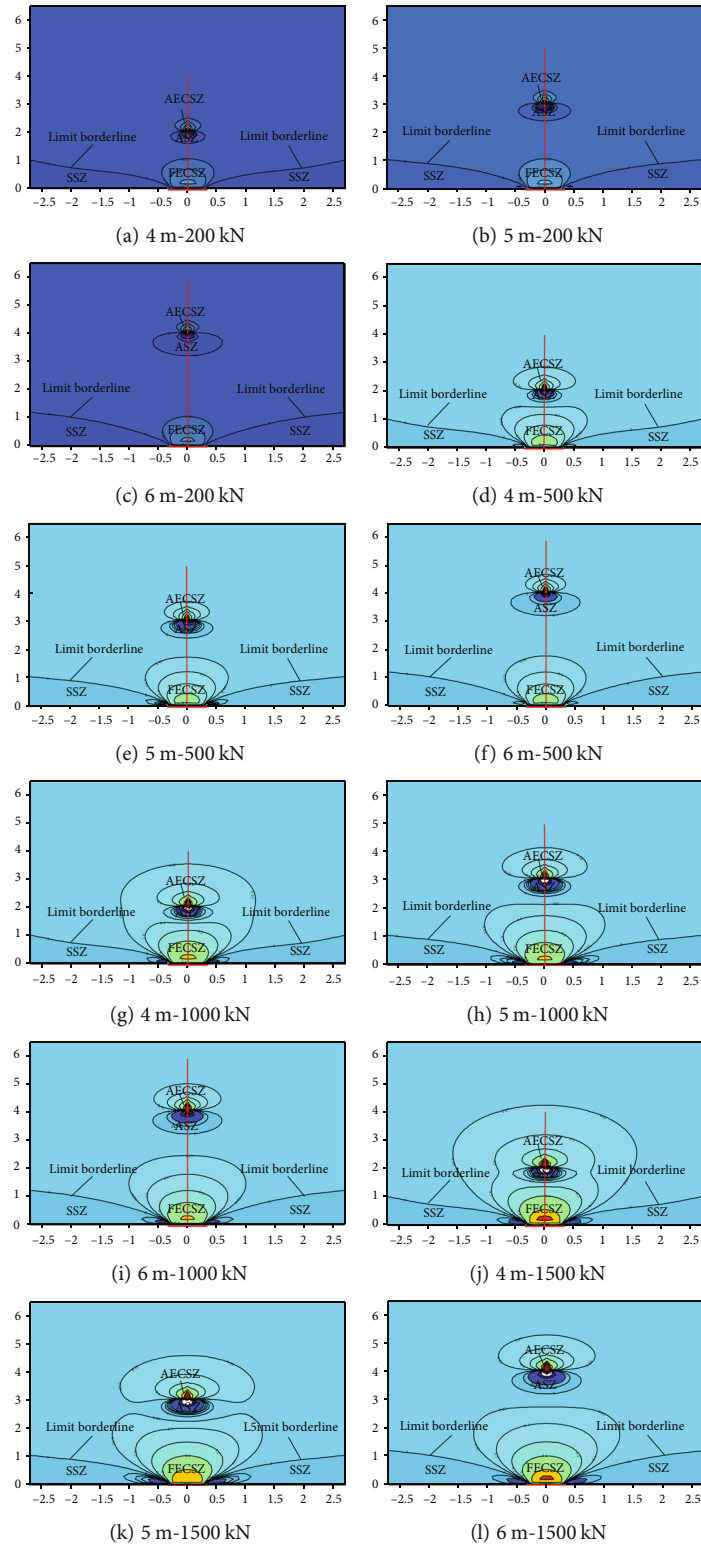


FIGURE 9: Continued.

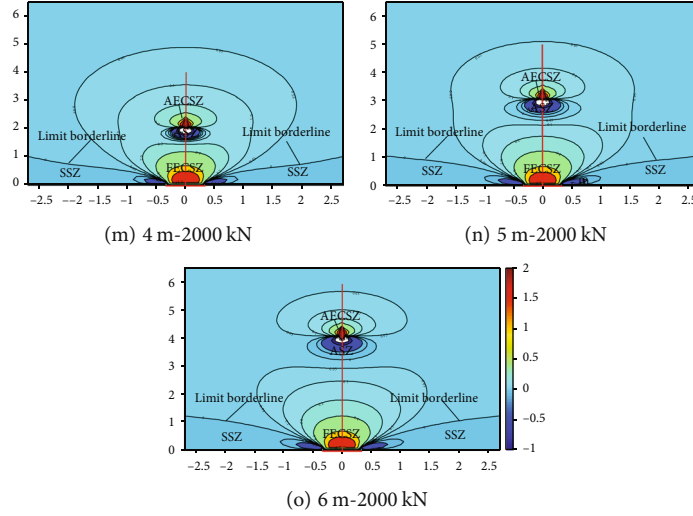


FIGURE 9: The results analysis of varying anchor length and prestress.

above results are simplified as follows.

$$M_{to}^V = M_{\sigma}^V(x, y, z, B_1) + M_{\sigma}^V(x, y, z, B_2) + \dots + M_{\sigma}^V(x, y, z, B_w), \quad (5)$$

$$M_{to}^H = M_{\sigma}^H(x, y, z, A_1) + M_{\sigma}^H(x, y, z, A_2) + \dots + M_{\sigma}^H(x, y, z, A_t). \quad (6)$$

Based on equations (5) and (6), the stress contour map of the interaction between the support bolt and the surrounding rock can be calculated. There are three key supporting mechanical parameters of a prestressed anchor: the initial prestress, P_0 ; the anchor length, L ; and the free section length, z_0 . This section calculates and analyzes the stressed states of the roof under varying prestresses, P_0 , and free lengths, L . The test parameters for the anchor are shown in Table 2.

Based on the above equations (1) and (5), the stress contour of the roof with different prestresses, P_0 , can be obtained, as shown in Figure 9. For ease of analysis, the range in which the compressive stress is greater than 0.05 MPa is defined as the effective compressive stress zone (ECSZ), and the range in which the stress is less than 0 MPa is defined as the special zone (SZ). The results show that there are two different ECSZs (Figures 9(a)–9(f), 9(h), 9(i), 9(k), 9(l), and 9(o)). One ECSZ is located in the anchoring section (this part is called AECSZ), and the other ECSZ is located in the free section (this part is called FECSZ). In addition, there are two different SZs. One SZ is located below the anchoring section (this part is called ASZ), and the other SZ is located near the surface of the surrounding rock (this part is called SSZ or dead zone). Among these SZs, the SSZ has a limit borderline inside the surrounding rock (Figures 9(a)–9(o)). When the free length, L , becomes longer, the borderline moves or expands slowly towards the inside of the roof, and the range of SSZ gradually becomes larger (Figures 9(a)–9(c), (Figures 9(g)–9(i), etc.). When the free length, L , is constant, it is interesting that

the position of the limit borderline and the range of the SSZ are constant regardless of the prestress. As the prestress of the anchor increases, the ranges of FECSZ, AECSZ, and ASZ gradually become larger, and the ranges of FECSZ and AECSZ get closer and finally blend (Figures 9(g), 9(j), 9(m), and 9(n)). In addition, the results show that the width of the ECSZ reduces in the X direction and the height of the FECSZ increases in the Z direction as the free length, L , increases. In this paper, the prestress of the anchor is called the ultimate prestress when the FECSZ and AECSZ are about to blend. Then, the critical prestresses of the 4 m and 5 m anchors are approximately 500 kN and 1500 kN, respectively (Figures 9(d) and 9(k)).

In this chapter, the key supporting parameters of a prestressed anchor bolt are studied by the analytical method, which provides the design basis for the support of deep, difficult surrounding rock. Unfortunately, the shear stress in the anchorage zone in the analytical method is fixed; in fact, the shear stress is variable in engineering, especially in the process of interface debonding. RFPA numerical simulation of shear stress variation can provide the basis for an analytical solution for anchor bolts. The in-depth integration analysis of the analytical method and the numerical simulation will continue in future work, which will provide references for improving the analytical method.

5. Conclusions

Most of the coal mine roadways are located in soft and broken-water-rich strata, and the roadway roof is very prone to instability and collapse under mining disturbance. This paper studies the law of stress evolution in the process of surrounding rock fracture and the relationship between surrounding rock fracture and prestressed anchor support. It also analyzes the mechanical properties of prestressed anchor bolt by analytical method and numerical simulation. Some conclusions are given below:

- (1) The change and attenuation of the surrounding rock stress have a certain influence on the stability of the

supporting bolt. The existence of confining pressure (horizontal stress) has a significant impact on the ultimate pullout force of anchor bolts. The higher the confining pressure stress, the greater the ultimate pullout force. When the confining stress of the surrounding rock reaches about 1 MPa, compared with the condition of 0 MPa, the ultimate bearing capacity of the anchor increases by about one time. The author believes that when the confining stress perpendicular to the anchor reaches about 1 MPa, the anchoring performance of the anchor can be well exerted

- (2) There is a critical, optimal value for the prestress of the anchor. For example, the anchor of a 4 m length (2 m free length) has a critical value of approximately 500 kN. In the anchor support design, the initial prestress of the anchor is recommended to be 40% of the critical value
- (3) When the prestressed anchor acts in the surrounding rock, there is a limit borderline, which is mainly related to the free length and the bonding length of the anchor and is not related to the prestress of the anchor. This result can predict the extent of the dead zone (SSZ) in roadway support
- (4) As the load increases, the de-bonded cracks in the anchorage interface expand continuously from the surface to the inside. After debonding, the interface shear stress tends to a low stable value, which means the value of friction resistance is relatively stable in different positions. In the numerical experiment (the bonding length is 300 mm), the ultimate drawing force of the anchor bolt is about 220 kN
- (5) The frictional resistance after interface debonding is an important condition to maintain the balance of the higher anchorage force. If there is no friction resistance, when the axial force of the anchor bolt reaches the initial critical value, the interface debonding process will develop catastrophically and cannot be stabilized until complete failure, even if the axial force no longer increases

Data Availability

Data can only be made available from the corresponding author.

Conflicts of Interest

The authors declare that they have no conflicts of interest.

Acknowledgments

This work was financially supported by the Foundation of State Key Laboratory of Public Big Data (no.PBD2022-18), China.

References

- [1] H. Fan, D. Zhao, J. Lai, and Y. Xie, "Water pressure and stress characteristics of lining structure in water rich karst tunnel," *IOP Conference Series: Earth and Environmental Science*, vol. 218, 2019.
- [2] D. W. Jin, "New development of water disaster prevention and control technology in China coal mine and consideration on methodology," *Coal Science and Technology*, vol. 45, no. 5, pp. 141–147, 2017.
- [3] P. Y. Li, "Mine water problems and solutions in China," *Mine Water and the Environment*, vol. 37, no. 2, pp. 217–221, 2018.
- [4] R. Pan, Q. Wang, B. Jiang et al., "Failure of bolt support and experimental study on the parameters of bolt-grouting for supporting the roadways in deep coal seam," *Engineering Failure Analysis*, vol. 80, pp. 218–233, 2017.
- [5] Y. Chen, Q. Meng, G. Xu, H. Wu, and G. Zhang, "Bolt-grouting combined support technology in deep soft rock roadway," *International Journal of Mining Science and Technology*, vol. 26, no. 5, pp. 777–785, 2016.
- [6] Q. Meng, L. Han, Y. Xiao, H. Li, S. Wen, and J. Zhang, "Numerical simulation study of the failure evolution process and failure mode of surrounding rock in deep soft rock roadways," *International Journal of Mining Science and Technology*, vol. 26, no. 2, pp. 209–221, 2016.
- [7] H. Kang, T. Jiang, and F. Gao, "Effect of protensioned stress to rock anchoring," *Journal of China Coal Society*, vol. 32, no. 7, pp. 432–448, 2007.
- [8] H. Kang, T. Jiang, and F. Gao, "Design of prestressed anchor support parameters," *Journal of China Coal Society*, vol. 33, no. 7, pp. 643–659, 2008.
- [9] H. Chen, C. H. Yang, D. Li, and B. W. Xia, "Model test study on mechanism of anchor in soft rock tunnel," *Chinese Journal of Rock Mechanics and Engineering*, vol. 28, pp. 2922–2927, 2009.
- [10] M. A. Meguid, O. Saada, M. A. Nunes, and J. Mattar, "Physical modeling of tunnels in soft ground: a review," *Tunnelling and Underground Space Technology*, vol. 23, no. 2, pp. 185–198, 2008.
- [11] J. Kemeny, "Time-dependent drift degradation due to the progressive failure of rock bridges along discontinuities," *International Journal of Rock Mechanics and Mining Sciences*, vol. 42, no. 1, pp. 35–46, 2005.
- [12] R. Wang, C. Li, J. Xu, and L. Pan, "Development and verification of large deformation model considering stiffness deterioration and shear dilation effect in FLAC^{3D}," *International Journal of Mining Science and Technology*, vol. 28, no. 6, pp. 959–967, 2018.
- [13] X. Sun, B. Zhang, L. Gan, Z. Tao, and C. Zhao, "Application of constant resistance and large deformation anchor cable in soft rock highway tunnel," *Advances in Civil Engineering*, vol. 2019, Article ID 4347302, 19 pages, 2019.
- [14] N. H. T. Nguyen, H. H. Bui, G. D. Nguyen, and J. Kodikara, "A cohesive damage-plasticity model for DEM and its application for numerical investigation of soft rock fracture properties," *International Journal of Plasticity*, vol. 98, pp. 175–196, 2017.
- [15] S. Chen, A. Wu, Y. Wang, X. Chen, R. Yan, and H. Ma, "Study on repair control technology of soft surrounding rock roadway and its application," *Engineering Failure Analysis*, vol. 92, pp. 443–455, 2018.
- [16] S. Zhang, T. Jiang, X. Pei et al., "A new forecasting method for failure time of creep landslide based on nonlinear creep

- behavior and new prewarning criterion," *Frontiers in Earth Science*, vol. 10, article 1018432, 2022.
- [17] S. Zhang, X. J. Pei, S. Y. Wang, R. Q. Huang, and X. C. Zhang, "Centrifuge model testing of loess landslides induced by excavation in Northwest China," *International Journal of Geomechanics*, vol. 20, no. 4, 2020.
- [18] S. Zhang, X. J. Pei, S. Y. Wang, R. Q. Huang, X. C. Zhang, and Z. L. Chang, "Centrifuge model testing of a loess landslide induced by rising groundwater in Northwest China," *Engineering Geology*, vol. 259, article 105170, 2019.
- [19] S. Zhang, X. C. Zhang, X. J. Pei et al., "Model test study on the hydrological mechanisms and early warning thresholds for loess fill slope failure induced by rainfall," *Engineering Geology*, vol. 258, article 105135, 2019.
- [20] X. J. Pei, S. Zhang, R. Q. Huang, K. H. Wei, F. Z. Liu, and Y. X. Duan, "Deformation propagation and identification of an impending disaster of a retained high embankment based on monitoring of minor deformation," in *Landslides and Engineered Slopes. Experience, Theory and Practice*, pp. 1583–1590, 2016.
- [21] M. C. He, J. L. Miao, and J. L. Feng, "Rock burst process of limestone and its acoustic emission characteristics under true-triaxial unloading conditions," *International Journal of Rock Mechanics and Mining Sciences*, vol. 47, no. 2, pp. 286–298, 2010.
- [22] S. Q. Yin, *Rock Mass Mechanics*, Mechanical Industry Press, 2012.
- [23] R. D. Mindlin, "Force at a point in the interior of a semi-infinite solid," *Physics*, vol. 7, pp. 195–199, 1936.
- [24] F. B. Zeng, *Calculation of Lateral Pressure on Rigid Wall when Uniform Load Acts on Rectangular Area*, J. Suzhou Insitute of Urban Construction and Environmental Protection, 1998.
- [25] P. F. Hu and Z. M. Zhang, "Integral of Mindlin's stress formula by mathematics software and its application," *Geotechnical Engineering Technique*, vol. 7, pp. 283–305, 2004.
- [26] M. Xiao, *The Study on the Mechanical Interaction of Anchor and Surrounding Rock*, Journal of China University of Mining and Technology, 2017.
- [27] H. T. Wang, Q. Wang, F. Q. Wang et al., "Mechanical effect analysis of bolts in roadway under different anchoring lengths and its application," *Journal of China Coal Society*, vol. 40, pp. 509–515, 2015.
- [28] Y. Cai, T. Esaki, and Y. Jiang, "A rock bolt and rock mass interaction model," *International Journal of Rock Mechanics and Mining Sciences*, vol. 41, no. 7, pp. 1055–1067, 2004.
- [29] H. F. Xu, B. Wang, M. Jiang, and Q. Tong, "Theoretical analysis of pullout deformation and stiffness of grouted rockbolts," *Chinese Journal of Geotechnical Engineering*, vol. 33, pp. 1511–1516, 2011.